Regenerative Engineering and Translational Medicine
https://doi.org/10.1007/s40883-024-00350-4

ORIGINAL RESEARCH

Photobiostimulation Enhances the Osteogenic Differentiation of Gingival-Derived Stem Cells Seeded on Nanocomposite Scaffolds

Eman Hany[1] · Ahmed A. Emam[2] · Mohamed G. Elbeltagy[3] · Mahmoud M. Zakaria[4] · Sarah Yahia[5] · Ibrahim M. El-Sherbiny[5] · Rana El-Qashty[1]

Received: 10 March 2024 / Revised: 11 April 2024 / Accepted: 27 June 2024

Abstract

Purpose This study was conducted to evaluate the effect of low-level laser therapy (LLLT) and cross-linked, nanofibrous, polycaprolactone/alginate scaffolds (PCL-NFs/Alg) on osteogenic differentiation of gingival mesenchymal stem cells (GMSCs) to develop a cell delivery system capable of enhancing bone regeneration.

Methods Rat GMSCs were isolated, and scaffolds were fabricated. A four-group study was designed; negative control (GMSCs + complete media), positive control (GMSCs + osteogenic supplement (OS)), scaffold (GMSCs/scaffold + OS), and scaffold/LLLT groups (GMSCs/scaffold + OS + LLLT). Diode laser LLLT was performed every 48 h. Samples were evaluated after 7 or 14 days. Cell proliferation was assessed using 3-(4,5-dimethylthiazol-2-yl)-2,5-diphenyltetrazolium bromide (MTT) assay. Mineralization and osteogenesis were evaluated by alizarin red S (ARS) and Von Kossa staining, beside real-time quantitative polymerase chain reaction (RT-qPCR), followed by statistical analysis.

Results For scaffold characterization, scanning electron microscopy confirmed the nanofibrous structure, EDX analysis showed signals of relevant elements, and FTIR spectrometry revealed the characteristic peaks of the polymeric constituents. Mechanical and water contact angle measurements reported improved results compared to the non-coated scaffolds. MTT assay revealed statistically significant increase in cell proliferation in scaffold/LLLT group. ARS and Von Kossa staining revealed the highest mineralization in scaffold/LLLT group. RT-qPCR showed significant increase in *OCN*, *ALP*, and *RUNX-2* expression in positive control, scaffold, and scaffold/LLLT groups respectively. However, *OPN* and *COL1a1* showed low expression levels.

Conclusion GMSCs have high osteogenic differentiation potential. Fabricated scaffolds possess good osteoconductive properties. LLLT significantly enhances cellular proliferation, and osteoblastic differentiation. Therefore, GMSCs-PCL/Alg-LLLT model can represent a promising choice for bone tissue engineering.

Lay Summary and Future Works A tissue engineering triad composed of GMSCs and nanofibrous PCL/Alg scaffold together with LLLT proved high potential for promoting cell proliferation, osteogenesis, and tissue mineralization in vitro. Experimental trials on animal bone defect models are required in future studies as a translational step towards clinical application of the constructed model.

Keywords Low-level laser therapy · Mesenchymal stem cells · Tissue engineering · Bone regeneration · Osteogenesis

Background

Bone injury that occurs as a result of diseases, trauma, infections, or after surgical tumor resection represents a great economic burden, as well as a medically challenging condition. Whereas small bone defects can heal on their own, large critical-sized defects can be difficult to restore. The most widely applied approach for large bone defect regeneration is grafting. However, this treatment modality can be compromised by the limited donor tissue, donor site morbidity, and risks of rejection or infection. Therefore, tissue engineering is arising as an alternative, more feasible solution [1].

Bone tissue engineering is a widely growing field that utilizes cells, scaffolds, and signaling molecules for the construction of biological substitutes for treating critical bone

Extended author information available on the last page of the article

Published online: 29 July 2024

defects [2]. Mesenchymal stem cells (MSCs) have the ability of self-renewal and differentiation into multiple cell lineages. They have been isolated from different oral and dental tissues including dental pulp, alveolar bone marrow, periodontal ligaments, apical papilla, dental follicle, periosteum, exfoliated deciduous teeth, salivary glands, oral epithelium, and gingival lamina propria [3]. Out of these types, gingival mesenchymal stem cells (GMSCs) represent the most easily accessible, abundant, and least invasive source of stem cells [4].

Developmentally, the gingival lamina propria, being derived from the neural cerst cells, has a dual origin: mesodermal and ectodermal [5]. This gives GMSCs the ability to differentiate into osteogenic, adipogenic, and chondrogenic as well as neural and endothelial cell lineages when cultured under proper conditions [6, 7]. GMSCs have the advantage of being homogenous and proliferating faster than bone marrow mesenchymal stem cells without the need for an exogenous growth factor. Importantly, GMSCs exhibit stable morphology and do not lose MSC characteristics at higher passages. In addition, GMSCs maintain normal karyotype and telomerase activity in long-term cultures, and are not tumorigenic [8].

GMSCs were reported to have anti-inflammatory and immunomodulatory effects [9], besides high proliferation capacity, multilineage differentiation, and osteogenic potentials which makes them a promising source for bone regeneration [7].

Scaffolds are the main actors in bone tissue engineering, where they support cellular attachment, proliferation, and osteo-differentiation [10]. Polycaprolactone (PCL) is a synthetic, semi-crystalline, aliphatic polyester that has been investigated as a prospective biomaterial for orthopedic applications due to its biocompatibility and slow degradation kinetics [11]. Moreover, alginate (Alg), which is derived from brown seaweed, is a well-known anionic linear natural polysaccharide that has been widely applied as a tissue regenerative material because it accelerates epithelialization and granular tissue formation, as well as encapsulating various growth factors [12]. In addition, calcium ionic cross-linking, which is one of the most commonly used ions, was found to prevent polymer dissolving in body fluids maintaining better stability for the scaffold [13].

In previous studies, calcium chloride ($CaCl_2$) cross-linked PCL/Alg nanocomposite scaffolds were evaluated in tissue engineering and resulted in osteo-induction of adipose-derived MSCs when co-cultured in vitro with osteogenic supplement media [14]. Moreover, in another in vivo study, when this scaffold was applied in class II furcation defects, it enhanced periodontal tissue regeneration [15].

Low-level laser therapy (LLLT) is based on the use of low-level lasers or light-emitting diodes to modulate cellular function. It refers to the application of lasers with a wavelength range of 600–1100 nm and an output power of 1–500 mW and relatively low-energy density (0.04–50 J/cm^2), and the laser can be directed to tissues or cultured cells [16]. The most important physiological benefit of LLLT is to increase the proliferation rate of cells [17]. In addition, it has an anti-inflammatory, analgesic, and reparative impact through enhancing the microcirculation, metabolism, and chemotaxis processes [18].

LLLT is a well-recognized tool in dentistry and regenerative medicine aiming to accelerate wound healing and manage functional disorders [19], where it regulates cellular functions by inducing cellular growth and cytokine release, hence exerting a variety of biological influences [20]. It has positive effects on cellular proliferation, endothelial cells' angiogenesis, and osteogenic differentiation, regulating fracture healing and bone regeneration [21].

Therefore, the present study was conducted to evaluate the effect of calcium chloride ($CaCl_2$) cross-linked PCL/Alg nanocomposite scaffolds on the proliferation and osteogenic differentiation of GMSCs with or without LLLT aiming to develop a tissue engineering complex capable of accelerating the healing process and regeneration of bone defects.

Materials and Methods

Study Design

Type of study: experimental randomized control trial.

Study groups:

Group I (negative control): GMSCs were cultured in complete media.
Group II (positive control): GMSCs were cultured in media with osteogenic supplement.
Group III (scaffold): GMSCs were seeded on scaffolds and cultured in media with osteogenic supplement.
Group IV (scaffold/LLLT): GMSCs were seeded on scaffolds, cultured in media with osteogenic supplement, and subjected to diode laser irradiation.

Scaffold Fabrication

Materials

Sodium alginate (SA), polycaprolactone (PCL), calcium chloride ($CaCl_2$), dichloromethane (DCM), and N,N-dimethylformamide (DMF) were purchased from Sigma-Aldrich (St. Louis, MO, USA).

Development of the Nanofibrous Multilayered Scaffold

Polycaprolactone nanofibrous scaffold (PCL-NFs) was developed via electrospining using NANON-01A electrospinning system, MECC Co., LTD followed by its coating with cross-linked Alg layers as described before in our previous study [22]. Briefly, a homogenous PCL solution (10% w/v) was prepared in a solvent mixture (DCM and DMF with a ratio of 60 and 40). Then, this solution was fed into a 13.1-mm plastic syringe and was exposed to a high voltage of 26 kV, fed rate of 4 mL/h, and tip-collector distance of 15 cm. The fabricated NFs were collected on the top of a metallic collector. After that, the prepared scaffold was dried in the vacuum oven overnight to remove the solvent residuals. The dried scaffold sheet was coated with SA aqueous solution (3% w/v) via the casting method from both sides and left to dry. The final scaffold was obtained via soaking the coated sheet in an aqueous solution of $CaCl_2$ (2% w/v) for just 2–3 min to cross-link the SA layers. The thickness of the final PCL-NFs/Alg fabricated sheets was 1.2–1.4 mm.

Scaffold Characterization

Morphological and Physical Analysis

For morphological and physical analysis, a scanning electron microscope (SEM; JSM-6510LV, JEOL, Tokyo, Japan) equipped with an energy-dispersive X-ray detector (EDX) was used. Square-shaped pieces of the scaffold sheets were cut, coated with gold, and examined. SEM micrographs were used to measure the fibers' average diameter. SEM examination was performed for the PCL-NFs layer before and after coating with Alg.

Chemical Analysis

A double-beam dispersive Fourier transform infrared (FTIR) spectrometer (Nicolet iS20, Thermo Electron Corporation, Warwickshire, UK) was utilized to detect the infrared spectra of the PCL-NFs and PCL-NFs/Alg scaffolds, as well as SA coating with 2 cm^{-1} resolution in a range of 500–4000 (cm^{-1}) performing a total of 100 scans.

Mechanical Analysis

The mechanical properties of the PCL-NFs and the final cross-linked PCL-NFs/Alg scaffold specimens were assessed using a universal testing machine (model 3345, Lloyd Testing Machine, England) at room temperature, accompanied with computer software (Nexygen 4.6, Lloyd Instruments Ltd. 2002, UK). Scaffold strips were prepared with average dimensions of 5×20 mm, then fixed vertically between two gripping units, with crosshead speed 10 mm/min and 5-KN load cell leaving a 4-mm gage length. Stress versus strain curves were analyzed, and tensile stress under maximal load was measured. Tensile properties were measured five times and average tensile strength was obtained.

Water Contact Angle Measurement

The water contact angle was measured for the PCL-NFs layer and the final cross-linked PCL-NFs/Alg scaffold. One drop of deionized water was dropped on the scaffold surface and a digital photo was taken, then after 10 s of dropping a water drop on the scaffold surface, the angle between the liquid surface and scaffold was calculated using ImageJ software (version 1.51r; NIH, Bethesda, MD, USA).

In Vitro Degradability and Water Absorption

Degradation and water absorption were assessed following previous protocols [23, 24]. Samples of equal sizes (5×5 mm) were immersed in equal amounts of phosphate-buffered saline (PBS) after initial weight determination (W0) and incubated at 37 °C. Scaffold samples were left for 1, 2, 4, or 6 weeks after which they were wiped, and wet weight was measured again (Ww). Samples were then finally dried in a lyophilizer (LABOCON LFD-BT-105, Leicester, UK) for 2 days and residual weight (Wr) was determined.

The water absorption (Wa) percentage was estimated through the following equation:

$$\mathrm{Wa}\,\% = \frac{\mathrm{Ww} - \mathrm{Wr}}{\mathrm{Wr}} \times 100$$

Weight loss (WL) percentage was estimated through the following equation:

$$\mathrm{WL}\,\% = \frac{\mathrm{W0} - \mathrm{Wr}}{\mathrm{W0}} \times 100$$

Isolation of Gingival-Derived Mesenchymal Stem Cells

Animal and cell culture procedures were performed at Mansoura Experimental Research Center (MERC, Mansoura University, Mansoura, Egypt). Six, male, healthy Sprague Dawley rats of 200–250 g weight (5–6 months of age) were euthanized by intraperitoneal injection of anesthetic overdose (sodium pentobarbital ≥ 0.86 mg/kg). Gingival tissue was collected from the posterior mandibular

gingiva, and then prepared according to the protocol described by Abd El-Latif et al. [25] (Fig. 1A). Briefly, gingival tissue samples were kept overnight in culture media containing dispase II (cat. #D4693, Sigma-Aldrich, St. Louis, MO, USA) to separate the epithelium. Then, connective tissue was minced into fragments and further digested with collagenase I (cat. #SCR103, EMD Millipore Corp, Burlington, MA, USA). The tissue explants were then incubated in Dulbecco Modified Eagle Medium (D-MEM) culture media (cat. #L0066-500) supplemented with 10% fetal bovine serum (FBS) (cat. #S1810-500), L-glutamine (cat. #P1012), and pencillin-streptomycin (cat. #100X-L0022) all purchased from BioWest, Nuaillé, France. The media was changed every 3 days. Cell cultures were evaluated each day by an inverted microscope (Olympus, CKX41SF, Tokyo, Japan) till reaching 80% confluence.

Osteogenic supplement media was prepared according to the protocol followed by Hanna et al. [26] using 100 nM dexamethasone (cat. #D4902), 200 µM L-ascorbic acid

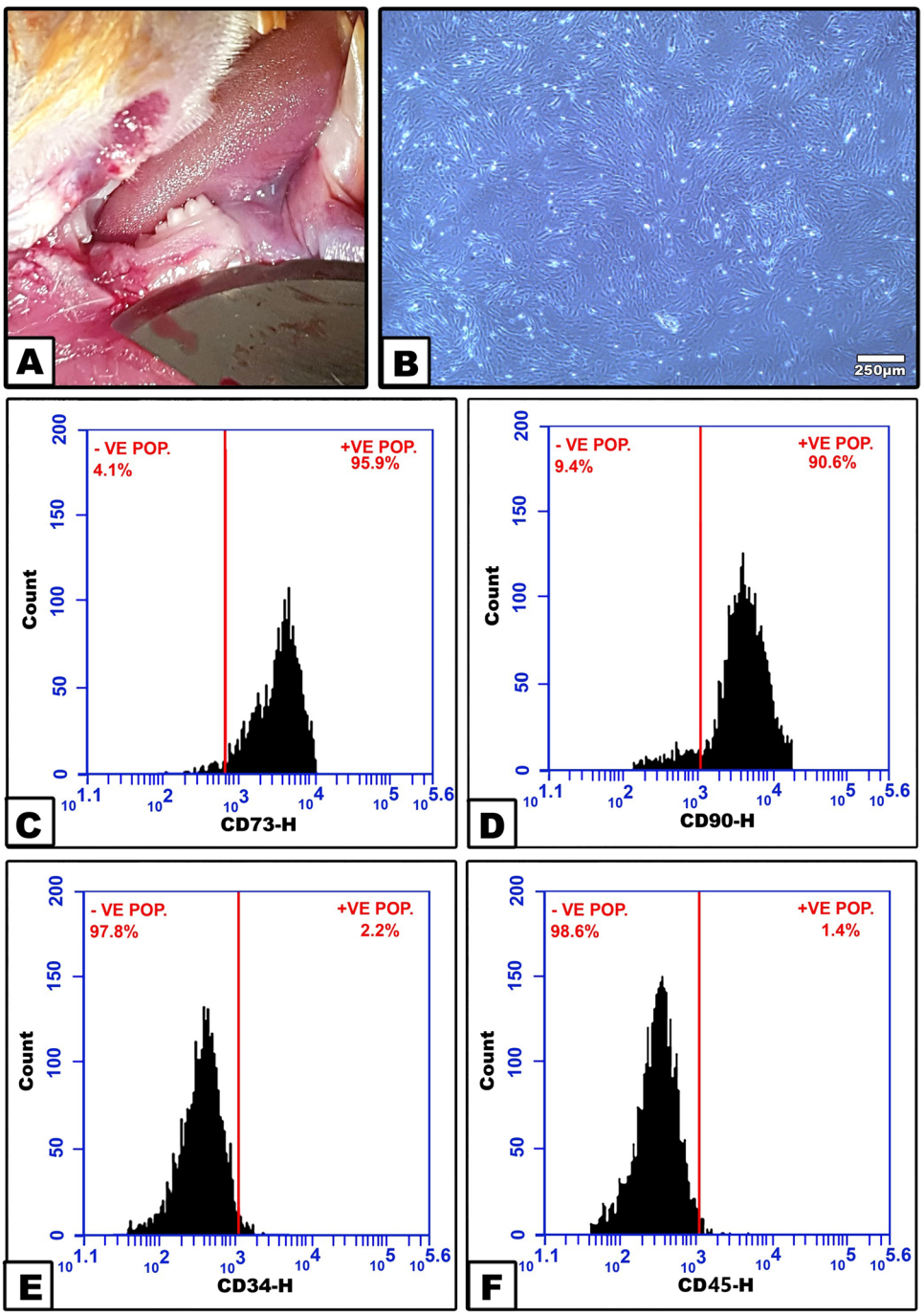

Fig. 1 **A** Surgical procedures for obtaining rat gingival tissue, **B** GMSC confluence, GMSC flowcytometric characterization histograms: **C** CD73, **D** CD90, **E** CD34, **F** CD45

2-phosphate (cat. #A8960), and 10 mM β-glycerol phosphate (cat. #50020) purchased from Sigma-Aldrich, Poole, UK.

Characterization of Gingival-Derived Mesenchymal Stem Cells

For GMSC characterization, a BD Accuri C6 flowcytometer (BD Biosciences, San Jose, CA, USA) and program software were used for flowcytometric immunophenotype determination. Third passage cells were treated with trypsin, followed by washing with PBS and incubation with the following primary antibodies; anti-CD90 PE (1:100; cat. #551,401), anti-CD73 purified (1:100; cat. #551,123), anti-CD45 FITC MAB (1:100; cat. #561,867) (all purchased from BD Biosciences, CA, USA), and anti-CD34 purified (R&D systems, 1:100; cat. #AF6518-SP, Minneapolis, MN, USA) using 10 µl/10^6 cells. For purified antibodies, fluorescein isothiocyanate fluorophores (FITC, cat. #F143, Thermo Fisher Scientific, Waltham, MA, USA) were added to each antibody, followed by their incubation in the dark for 30 min at 4 °C. PBS was then used to rinse the labeled GMSCs, which were then centrifuged for 5 min at 200 × g and suspended in PBS.

Seeding of Gingival-Derived Mesenchymal Stem Cells

Scaffold samples of 5 × 5 mm were sterilized with ethanol and ultraviolet light then incubated in culture media overnight. GMSCs (4×10^5) were seeded dropwise on top of each scaffold sample, placed in 6-well plates, and then left to seed. Culture media was added to the seeded scaffolds and incubated in an atmosphere of 5% CO_2. Media was changed every 2 days.

Photobiostimulation

Photobiostimulation was performed using Solase dental Diode laser (Lazon, Guangdong, China). Before irradiation, power output was measured by power meter. Culture plates containing the scaffolds seeded with GMSCs were wrapped with aluminum foil to reflect any irradiation and laser beam was applied through an opening in the aluminum foil. Irradiation was done in the biological safety cabinet to avoid contamination using the parameters described in Table 1.

Table 1 LLLT irradiation parameters

Active medium	InGaAs (semiconductor)
Wavelength	980 nm
Laser tip diameter	3 cm
Irradiation mode	Continuous
Power	0.2 W
Power density	0.03 W/cm^2
Energy	30 J
Energy density	4.24 J/cm^2
Duration	150 s over 2 sessions separated by 75 s
Distance	0.5 cm
Irradiation	Every 48 h for 7 or 14 days (3 or 7 sessions)

Cell Proliferation Assay

Cell viability and proliferation in negative control and scaffold and scaffold/LLLT groups were assessed on days 1, 3, and 5 using 3-(4,5-dimethylthiazol-2-yl)-2,5-diphenyltetrazolium bromide (MTT) colorimetric assay (cat. #M6494, Thermo Fisher scientific, Carlsbad, CA, USA). Briefly, culture media was removed, and cells were incubated with MTT reagent (0.5 µg/mL) for 2 h at 37 °C. For dissolving formazan crystals, dimethyl sulfoxide (DMSO) was added, and after incubation for 30 min, the absorbance was measured at 550 nm using a microplate reader (Biotek, ELx800, Winooski, VT, USA).

Alizarin Red S (ARS) Staining

Alizarin red S staining was used to assess mineralization in the cell matrix at days 7 and 14 as described in a previous study [22] where ARS is widely used as the gold standard for the detection of cell mineralization [27]. Briefly, the culture media was discarded, and cells were washed with PBS containing Ca/Mg, fixed, and washed again. The cells were then incubated with ARS (cat. #A5533, Sigma-Aldrich) (40 mM in deionized water, pH 4.2) for 45 min after which they were washed, and PBS was added. For quantification of deposits, the stained cells were dissolved in 10% acetic acid for 45 min after which they were washed, and PBS was added. Cultures were observed and photographed with an inverted microscope and the degree of absorbance was measured by a microplate reader (Biotek, ELx800).

Von Kossa Staining

Von Kossa staining was carried out to detect mineralization in the cell cultures at days 7 and 14 according to the protocol by Ball et al. [28] where Von Kossa is used to detect the calcium binding sites by replacing calcium by silver ions [29]. In brief, GMSCs were fixed, washed, and then incubated with 5% silver nitrate ($AgNO_3$) (cat. #209139, Sigma-Aldrich) under UV light, for 45 min. $AgNO_3$ solution was then aspirated and the cells were washed three times with distilled water (dH_2O). Five percent sodium carbonate (Na_2CO_3) (cat. #S263-500, Thermo Fisher Scientific) in 10% formalin (Fisher Scientific) was then added for 4 min followed by rinsing twice with dH_2O. The stain was

fixed with 5% sodium thiosulfate ($Na_2S_2O_3$) (cat. #217263, Sigma-Aldrich) for 2 min followed by rinsing twice with dH_2O. Cultures were observed and photographed with an inverted microscope.

Reverse Transcription and Real-Time Quantitative Polymerase Chain Reaction (RT-qPCR)

Total RNA was isolated from GMSCs using Direct-zol RNA Miniprep (cat. # R2051, zymoresearch, Irvine, CA, USA) supplied with TRI Reagent (cat. #R2050-1–50) according to the manufacturer's instruction. COSMO cDNA synthesis kit (cat. #WF10205001, Willowfort, Birmingham, UK) was used for reverse transcription of total RNA. RT-qPCR reaction was performed for amplification of the cDNA using HERA PLUS SYBR® Green qPCR Kit (cat. #WF10308001, Willowfort, Birmingham, UK) in a real-time thermal cycler (Thermo Fisher Scientific, Vantaa, Finland).

RT-qPCR reaction was performed with 20 µL; 10 µL of SYBR Green, 2 µL of forward and reverse primers, 1 µL of cDNA, and 7 µL of RNase-free water. RT-qPCR cycling stages were carried out as follows: initial denaturation for 10 min at 95 ℃, 40 cycles of denaturation for 15 s at 95 ℃, annealing for 30 s at 60 ℃, and extension for 30 s at 72 ℃.

Expression levels of osteoblast-specific mRNA target genes collagen 1α1 (*COL1α1*), osteocalcin (*BGLAP*) (*OCN*), osteopontin (*SPP1*) (*OPN*), alkaline phosphatase (*ALP*), and Runt-related transcription factor 2 (*RUNX2*) were detected. Glyceraldehyde-3 phosphate dehydrogenase (*GAPDH*) was used as a housekeeping gene. All primers were purchased from Vivantis Technologies (Selangor Darul Ehsan, Malaysia). The primer sequences utilized in this study are listed in Table 2.

Statistical Analysis

Sample size was calculated by G*Power software (version 3.1.9.7). Based on a previous study [22], we hypothesized a large effect size ($f = 0.8$) for a factorial design with two factors at 2 and 3 levels, i.e., 6 cells (intervention combinations). A total of 24 units were required to provide 4 units per cell. This design achieves 96% power when an F test is used to test factor A (groups with 4 levels) at a 5% significance level and the effect size is 0.800, achieves 91% power when an F test is used to test factor B (time with 2 levels) at a 5% significance level and the effect size is 0.800, and achieves 91% power when an F test is used to test the A*B interaction at a 5% significance level and the effect size is 0.800.

Data was entered and analyzed using IBM-SPSS software (IBM Corp. Released 2020. IBM SPSS Statistics for Windows, Version 27.0. Armonk, NY, USA: IBM Corp). Quantitative data were initially tested for normality using Shapiro–Wilk's test and homogeneity of variances was assessed by Levene's test. The presence of significant outliers was tested by inspecting boxplots. Quantitative data were expressed as median (Q1–Q3) and compared between multiple groups using Kruskal–Wallis *H*-test or mean ± SD and compared for two-factors (group and time) using two-way analysis of variance (ANOVA). For any of the used tests, results were considered as statistically significant if p value ≤ 0.05, or according to Bonferroni correction when doing multiple tests' comparisons.

Results

Scaffold Characterization Results

Morphological and Physical Analysis

The surface morphology of the developed scaffolds showed a nanofibrous structure with an average diameter of around 307.2–2400 nm for PCL-NFs and 265–611 nm for PCL-NFs/Alg scaffolds (Fig. 2A, B). The EDX analysis of the fabricated scaffold showed signals corresponding

Table 2 Primer sequences for qPCR

	Gene	Primers	Sequence
1	Alkaline phosphatase	Alpl-F	GAC AAG AAG CCC TTC ACA GC
		Alpl-R	ACT GGG CCT GGT AGT TGT TG
2	RUNX2	Runx2-F	GGA CGA GGC AAG AGT TTC AC
		Runx2-R	GGA CCG TCC ACT GTC ACT TT
3	Osteocalcin	Bglap-F	GAG GGC AGT AAG GTG GTG AA
		Bglap-R	GTC CGC TAG CTC GTC ACA AT
4	Osteopontin	Spp1-F	GAT CGA TAG TGC CGA GAA GC
		Spp1-R	ACT CGT GGC TCT GAT GTT CC
5	Collagen 1α1	Col1α1-F	CTG GTG AAC AGG GTG TTC CT
		Col1α1-R	GGA AAC CTC TCT CGC CTC TT
6	GAPDH	Gapdh-F	TGG GAA GCT GGT CAT CAA C
		Gapdh-R	GCA TCA CCC CAT TTG ATG TT

to the elements C, O, Na, Cl, and Ca with weight percentages of 51.75, 32.68, 5.82, 8.49, and 1.26%, respectively, which coincides with the structure of the fabricated scaffold (Fig. 2C).

Chemical Analysis

FTIR spectrometric analysis revealed all the characteristic peaks of the polymeric constitutes of the developed nanofibrous multilayered scaffold. The characteristic peaks of

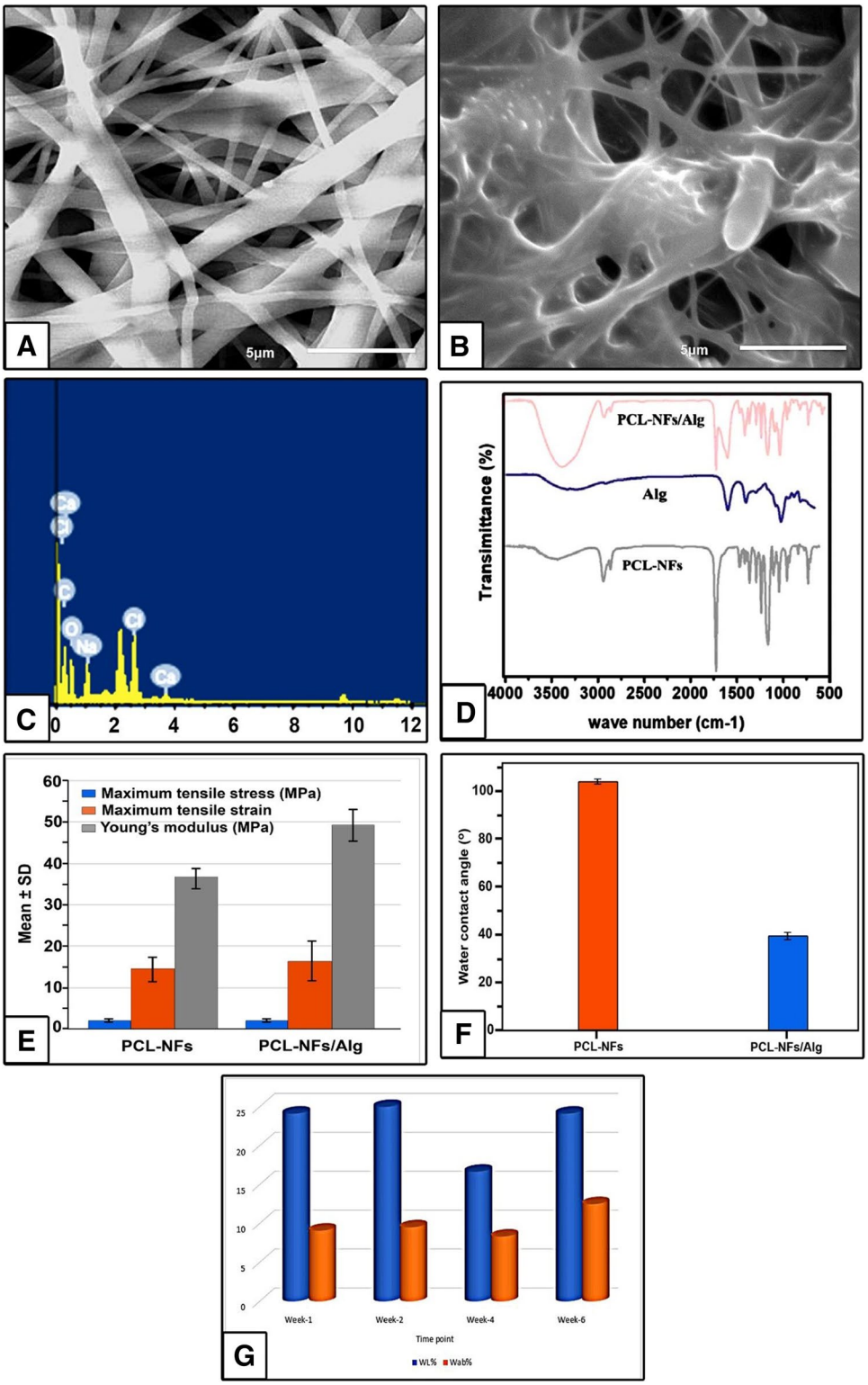

Fig. 2 Scaffold characterization. **A** SEM micrographs of the PCL-NFs scaffold. **B** SEM micrographs of crosslinked PCL-NFs/Alg scaffold. **C** Energy-dispersive X-ray (EDX) analysis. **D** FTIR of the developed scaffolds. **E** Mechanical properties of scaffolds. **F** Water contact angle measurements. **G** Weight loss and water absorption percentages

PCL and alginate appeared in the spectrum of the fabricated scaffold. PCL-related peaks appeared at 2862 cm^{-1} and 2939 cm^{-1} for symmetric and asymmetric stretching of υCH_2 respectively. Another intense peak was observed at 1718 cm^{-1} and attributed to the stretching vibration of ester [amid I UC = O]. In addition, peaks related to alginate were detected at 2928 cm^{-1} related to the CH_2 stretching and at 1597.3 cm^{-1} that is corresponding to the carbonyl group (C = O) [30–32] (Fig. 2D).

Mechanical Tests

Cross-linked PCL-NFs/Alg scaffold attained higher values of maximum tensile stress and strain as compared to non-coated scaffolds. Moreover, the coating of PCL-NFs with Alg improved its elastic modulus significantly from 37.1 ± 2.35 to 49.53 ± 3.85 MPa. Similar studies showed high mechanical properties of different PCL/Alg-based scaffolds [33, 34]. In addition, the ultimate strain value of the developed scaffolds was similar to the normal bone range (2–30%) as reported by Osterhof et al. [35] (Fig. 2E).

Water Contact Angle

Water contact angle measurement illustrated the hydrophobic nature of the developed PCL-NFs scaffold which attained higher value of water contact angle around $103.55 \pm 0.89°$. In contrast, this value was significantly decreased after coating the PCL-NFs from both sides with Alg to $39.54 \pm 1.25°$. This reduction was attributed to increasing the hydrophilicity of the fabricated nanofibers by Alg outer layers (Fig. 2F).

In Vitro Degradation and Water Absorption

Kruskal–Wallis *H*-test was performed for weight loss and water absorption percentages and showed no statistically significant difference in WL% or Wab% between the four time points (Fig. 2G) (Table 3).

Gingival-Derived Mesenchymal Stem Cells' Characterization Results

GMSCs showed typical spindle, fibroblast-like morphology, and adherence to plastic walls (Fig. 1B). Third passage cells were subjected to cell surface phenotypic marker analysis where the mesenchymal markers CD73 (95.9%) and CD90 (90.6%) were found to be highly positive, while the hematopoietic markers CD34 (2.2%) and CD45 (1.4%) were negative (Fig. 1C–F).

Cell Proliferation Assay Results

A two-way ANOVA was conducted to examine the effects of group and time on cellular proliferation through the MTT assay. Residual analysis was performed to test for the assumptions of the two-way ANOVA. There were no significant outliers, residuals were approximately normally distributed ($p > 0.05$), and there was homogeneity of variances ($p > 0.05$).

This parameter involved 9 units divided by two factors as follows: grouping factor—3 groups, 3 units per group (negative control, scaffold, and scaffold/LLLT); and time factor—3 time points, 9 units per time point (1 day, 3 days, and 5 days).

Cellular proliferation as detected by MTT assay showed higher mean values in the scaffold/LLLT group, followed by the scaffold and then the control groups respectively at each time point as well as time-dependent increase through days 1, 3, and 5 in each group (Fig. 3A) (Table 4). Statistical analysis showed a statistically significant interaction between group and time on MTT. Therefore, an analysis of simple main effects for each factor was performed with statistical significance receiving a Bonferroni adjustment and being accepted at the $p < 0.0167$ level.

As regards the simple main effect for group, there was a statistically significant difference in mean "MTT" values between the groups at 3- and 5-day time points [$F(2, 18) = 1.479$, $p = 0.254$, partial $\eta^2 = 0.141$ at day 1; $F(2, 18) = 3.968$, $p = 0.037$, partial $\eta^2 = 0.306$ at day 3; and $F(2, 18) = 30.941$, $p < 0.001$, partial $\eta^2 = 0.775$ at day 5].

Table 3 Weight loss and water absorption percentages in the four time points

Parameter	Time point				Test of significance	
	Week 1	Week 2	Week 4	Week 6	*H* [3]	*p*-value
WL%	24.14 (8.79–33.90)	25 (14.79–27.72)	16.67 (13.4–33.68)	24.14 (18.57–34.82)	1.042	0.791
Wab%	9.09 (6.43–18.68)	9.52 (5.7–17.36)	8.33 (5.12–23.1)	12.5 (6.47–40.79)	1.394	0.707

WL weight loss, *Wab* water absorption. Data is median (Q1–Q3). The test of significance is the Kruskal–Wallis *H*-test

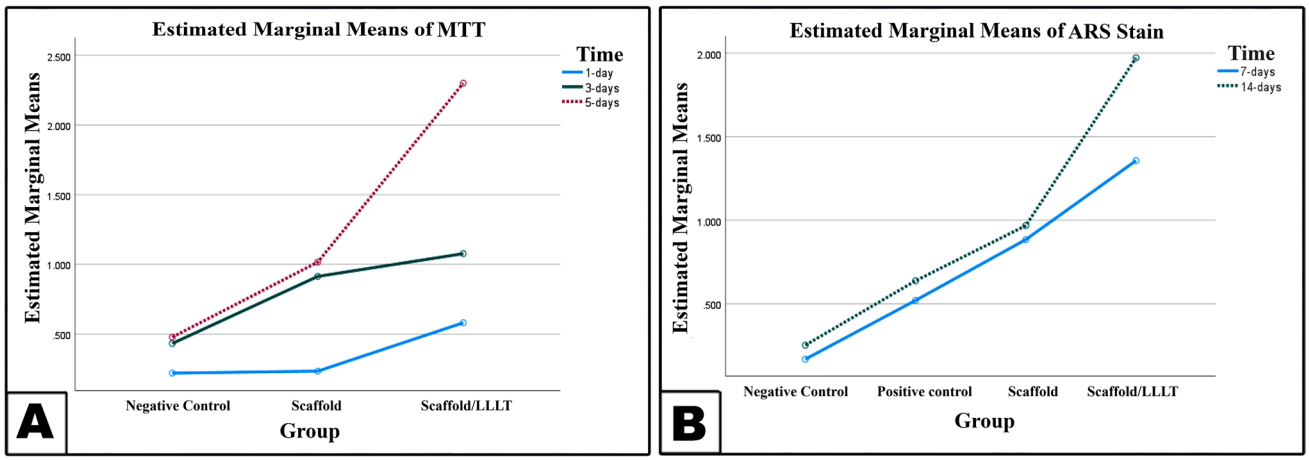

Fig. 3 Line graphs showing the mean values for **A** MTT assay, **B** ARS staining

Therefore, pairwise comparisons were run for simple main effects at 3 and 5 days. At 3 days, pairwise comparisons revealed a statistically significant difference between the control group vs. scaffold/LLLT group ($p=0.043$), but not between the control vs. scaffold group ($p=0.174$), or scaffold vs. scaffold/LLLT groups ($p=1.000$). At 5 days, there was a statistically significant difference ($p<0.001$) between scaffold/LLLT vs. control and scaffold groups, but not between control vs. scaffold ($p=0.109$).

As regards the simple main effect for time, there was a statistically significant difference in mean values between the three time points in scaffold and scaffold/LLLT groups but not in the control group [$F(2, 18)=0.669$, $p=0.525$, partial $\eta^2=0.069$ in control; $F(2, 18)=6.384$, $p=0.008$, partial $\eta^2=0.415$ in scaffold; and $F(12, 18)=27.634$, $p=<0.001$, partial $\eta^2=0.754$ in scaffold/LLLT groups]. Therefore, pairwise comparisons were run for simple main effects in scaffold and scaffold/LLLT groups only. In the scaffold group, pairwise comparisons revealed a statistically significant difference between day 1 vs. day 3 ($p=0.031$), and day 1 vs. day 5 ($p=0.012$), but not between day 3 vs. day 5 ($p=1.000$). In the scaffold/LLLT group, pairwise comparisons revealed a statistically significant difference between day 5 vs. day 1 ($p<0.001$), and day 5 vs. day 3 ($p<0.001$), but not between day 1 vs. day 3 ($p=0.155$).

Alizarin Red S Staining Results

This study involved 24 units divided by two factors as follows: grouping factor—4 groups, 6 units per group (negative control, positive control, scaffold, and scaffold/LLLT); and time factor—2 time points, 12 units per time point (7 days and 14 days). Mineralization as detected by ARS showed higher values in the scaffold/LLLT group, followed by the scaffold and then the positive and negative control groups respectively at each time point, as well as time-dependent increase through days 7 and 14 in each group (Figs. 3B, 4A–D, A1–D1) (Table 5).

There was a statistically significant interaction between group and time on mineralization levels as detected by ARS stain. Therefore, an analysis of simple main effects for each factor was performed with statistical significance receiving a Bonferroni adjustment and being accepted at the $p<0.008$ level.

As regards the simple main effect for group, there was a statistically significant difference in mean values between the four groups at each time point [$F(3, 16)=98.204$, $p<0.001$, partial $\eta^2=0.948$ at 7-day time point, and $F(3, 16)=206.128$, $p<0.001$, partial $\eta^2=0.975$ at 14-day time point]. At 7 days, all pairwise comparisons revealed a

Table 4 MTT results according to group and time with their interaction

Time	Group			Test of significance		
	Control	Scaffold	Scaffold/LLLT	*F*	*p*-value	Partial η^2
At day 1	0.220 ± 0.033	0.234 ± 0.016	0.581 ± 0.105	6.143	**0.003**	0.577
At day 3	0.432 ± 0.056	0.914 ± 0.575	1.077 ± 0.335			
At day 5	0.478 ± 0.139	1.016 ± 0.504	2.300 ± 0.185			

Data is presented as mean ± SD. The test of significance is two-way ANOVA. Partial η^2 is a measure of effect size

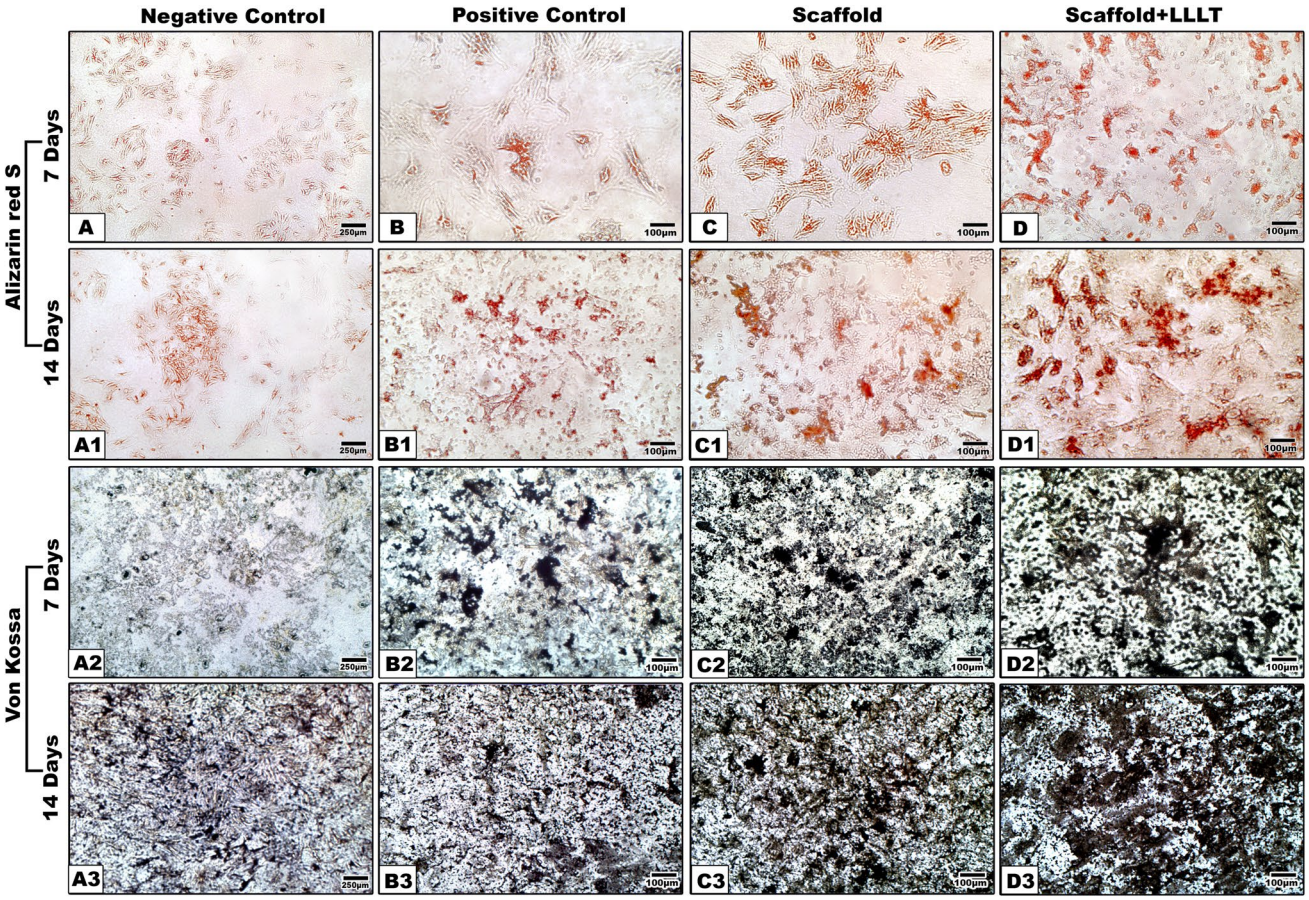

Fig. 4 Photomicrographs of alizarin red S and Von Kossa staining of different groups at different time points

statistically significant difference ($p = 0.001$ for negative vs. positive control, and < 0.001 for other pairwise comparisons). At 14 days, all pairwise comparisons revealed a statistically significant difference ($p = 0.002$ for positive control vs. scaffold and < 0.001 for other pairwise comparisons).

As regards the simple main effect for time, there was a statistically significant difference in mean values between the 2 time points in scaffold/LLLT group only being higher at 14 days vs. 7 days [$F(1, 16) = 1.339$, $p = 0.264$, partial $\eta^2 = 0.077$ in negative control group, $F(1, 16) = 2.612$, $p = 0.126$, partial $\eta^2 = 0.140$ in positive control group, F(1, 16) = 1.328, $p = 0.266$, partial $\eta^2 = 0.077$ in scaffold group, and $F(1, 16) = 71.842$, $p = < 0.001$, partial $\eta^2 = 0.818$ in scaffold/LLLT group].

Von Kossa Staining Results

By Von Kossa staining, calcified nodules stained black. In negative control groups, minimal mineralization could be detected, while in the other groups, calcified deposits were detected with the scaffold/LLLT group showing notably the highest calcification regarding area and number of nodules, followed by the scaffold group, then the positive control group (Fig. 4A2–D2, A3–D3).

Table 5 ARS stain results according to group and time with their interaction

Time	Group				Test of significance		
	Negative control	Positive control	Scaffold	Scaffold/LLLT	F	*p*-value	Partial η^2
ARS dye					12.890	**< 0.001**	0.707
7 days	0.169 ± 0.009	0.521 ± 0.091	0.885 ± 0.018	1.357 ± 0.217			
14 days	0.253 ± 0.050	0.638 ± 0.041	0.968 ± 0.048	1.973 ± 0.035			

Data is presented as mean ± SD. The test of significance is two-way ANOVA. Partial η^2 is a measure of effect size

RT-qPCR Statistical Analysis Results

Concerning the mean values for ALP, RUNX2, and OCN gene expression, it was observed that the scaffold/LLLT group showed the highest values followed by the scaffold, positive control, and negative control groups which showed the least expression at both time intervals. Moreover, the 14-day time point showed higher gene expression as compared to the 7 days for all groups. However, *OPN* and *COL1α1* showed low expression levels (Fig. 5) (Table 6).

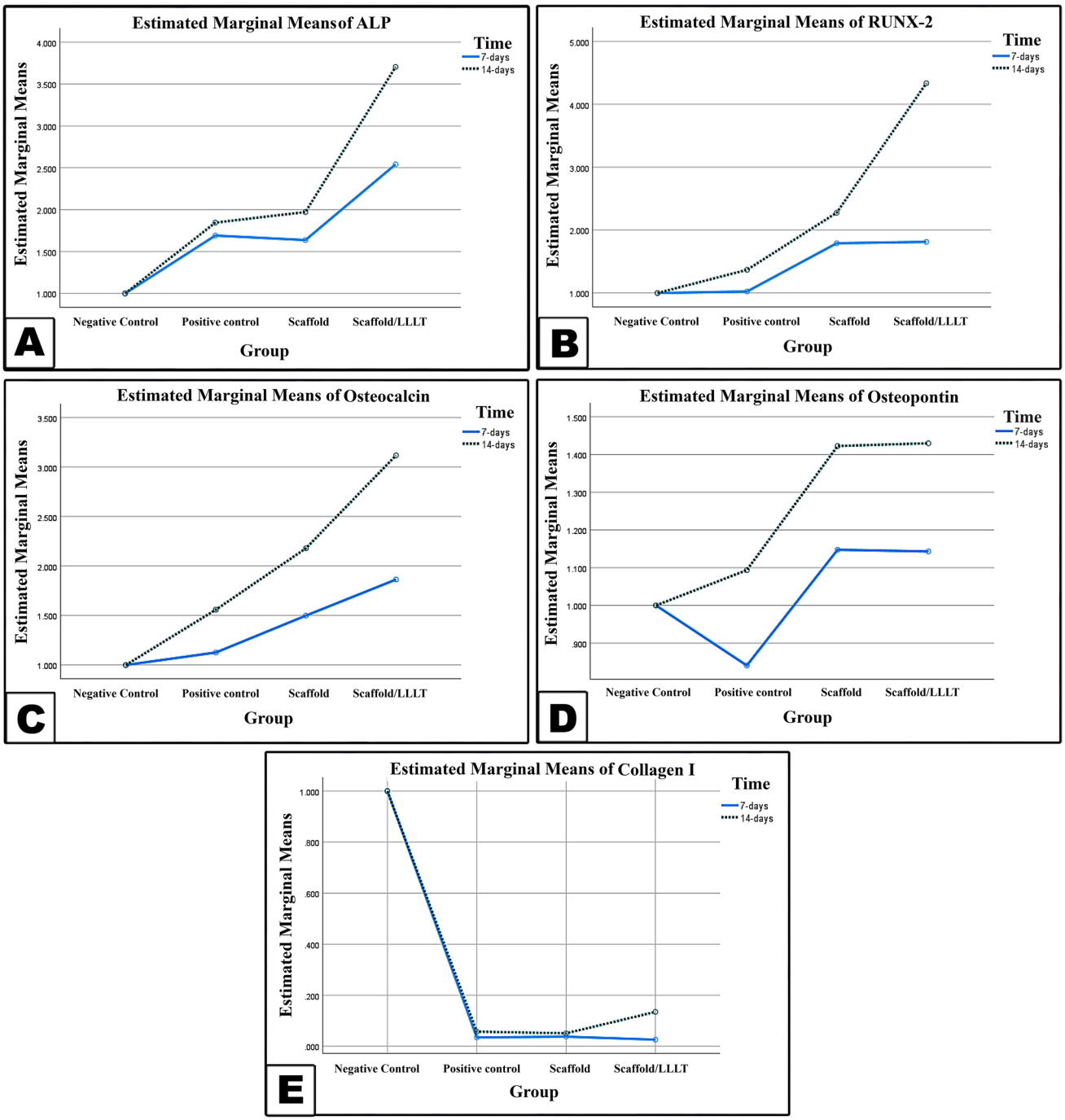

Fig. 5 Line graphs showing the mean values for RT-PCR results. **A** Alkaline phosphatase. **B** Runx-2. **C** Osteocalcin. **D** Osteopontin. **E** Collagen1

Table 6 PCR results according to group and time with their interaction

Time	Group				Test of significance		
	Negative control	Positive control	Scaffold	Scaffold/LLLT	F	*p*-value	Partial η2
ALP					1.647	0.218	0.236
7 days	1 ± 0	1.591 ± 0.094	1.637 ± 0.042	2.541 ± 0.752			
14 days	1 ± 0	1.846 ± 0.324	1.972 ± 0.735	3.704 ± 0.858			
Runx2					4.421	**0.019**	0.453
7 days	1 ± 0	1.025 ± 0.102	1.792 ± 0.717	1.813 ± 0.505			
14 days	1 ± 0	1.370 ± 0.180	2.278 ± 0.961	4.336 ± 1.341			
Osteocalcin					2.292	0.117	0.301
7 days	1 ± 0	1.127 ± 0.347	1.499 ± 0.356	1.864 ± 0.716			
14 days	1 ± 0	1.559 ± 0.484	2.180 ± 0.537	3.118 ± 0.391			
Osteopontin					0.191	0.901	0.034
7 days	1 ± 0	0.841 ± 0.663	1.148 ± 0.043	1.143 ± 0.072			
14 days	1 ± 0	1.094 ± 0.579	1.423 ± 0.578	1.430 ± 0.244			
Collagen1					9.970	**< 0.001**	0.651
7 days	1 ± 0	0.035 ± 0.014	0.038 ± 0.037	0.026 ± 0.016			
14 days	1 ± 0	0.058 ± 0.017	0.051 ± 0.020	0.135 ± 0.021			

Data is presented as mean ± SD. The test of significance is two-way ANOVA. Partial η^2 is a measure of effect size

Alkaline Phosphatase

There was no statistically significant interaction between group and time on *ALP* gene expression. Therefore, an analysis of the main effects for each factor was reported.

As regards the main effect for group, there was a statistically significant difference in mean values between the four groups [$F(3) = 19.044$, $p < 0.001$, partial $\eta^2 = 0.781$]. Mean ± SE was lower in negative control (1 ± 0.202) < positive control (1.768 ± 0.202) < scaffold (1.805 ± 0.202) < scaffold/LLLT (3.123 ± 0.202) groups. The pairwise comparisons revealed a statistically significant difference between negative control vs. scaffold ($p < 0.001$), positive control vs. scaffold/LLLT ($p = 0.001$), and scaffold vs. scaffold/LLLT ($p = 0.001$), but there was no statistically significant difference for all other pairwise comparisons (negative vs. positive control ($p = 0.069$), negative control vs. scaffold ($p = 0.054$), and positive control vs. scaffold/LLLT ($p = 0.999$)).

As regards the main effect for time, there was no statistically significant difference tween the 2 time points [$F(1) = 4.184$, $p = 0.058$, partial $\eta^2 = 0.207$]. However, mean ± SE was higher at 14 days (0.130 ± 0.143) vs. 7 days (1.717 ± 0.143) (Fig. 5A).

RUNX2 There was a statistically significant interaction between group and time on *RUNX2* gene expression. Therefore, an analysis of simple main effects for each factor was performed with statistical significance receiving a Bonferroni adjustment and being accepted at the $p < 0.008$ level.

As regards the simple main effect for group, there was a statistically significant difference in mean *RUNX2* values between the 4 groups at 14 days but not at 7 days [$F(3, 16) = 15.136$, $p < 0.001$, partial $\eta^2 = 0.739$ at 14-day time point, and $F(3, 16) = 0.414$, $p = 0.275$, partial $\eta^2 = 0.210$ at 7 days]. Therefore, pairwise comparisons were run for simple main effect at 14 days only and revealed a statistically significant difference ($p < 0.001$) between negative control vs. scaffold, and positive control vs. scaffold as well as between scaffold vs. scaffold/LLLT ($p = 0.010$), but not between negative vs. positive control ($p = 1.0$), negative control vs scaffold/LLLT ($p = 0.190$), and positive control vs scaffold/LLLT groups ($p = 0.682$).

As regards the simple main effect for time, there was a statistically significant difference in mean values between the 2 time points in scaffold/LLLT group only being higher at 14 days vs. 7 days [$F(1, 16) = 0.000$, $p = 1.000$, partial $\eta^2 = 0.000$ in negative control group; $F(1, 16) = 0.403$, $p = 0.534$, partial $\eta^2 = 0.025$ in positive control; $F(1, 16) = 0.8011$, $p = 0.384$, partial $\eta^2 = 0.048$ in scaffold group, and $F(1, 16) = 21.597$, $p = < 0.001$, partial $\eta^2 = 0.574$ in scaffold/LLLT group] (Fig. 5B).

Osteocalcin

There was no statistically significant interaction between group and time on *OCN* gene expression. Therefore, an analysis of the main effects for each factor was reported.

As regards the main effect for the group, there was a statistically significant difference in mean *OCN* values between the 4 groups [$F(3) = 14.034$, $p < 0.001$, partial $\eta^2 = 0.725$.

Mean ± SE was lower in negative control (1 ± 0.173) < positive control (1.343 ± 0.173) < scaffold (1.839 ± 0.173) < scaffold/LLLT groups (2.491 ± 0.173). The pairwise comparisons revealed a statistically significant difference between negative control vs. scaffold ($p = 0.016$) and scaffold/LLLT ($p < 0.001$), as well as positive control vs. scaffold/LLLT ($p < 0.001$), but no significant difference for all other pairwise comparisons [negative vs. positive control ($p = 0.516$), positive control vs. scaffold ($p = 0.218$), and scaffold vs. scaffold/LLLT groups ($p = 0.072$).

As regards the main effect for time, there was a statistically significantly higher *OCN* expression at 14 days vs. 7 days [$F(1) = 11.714$, $p = 0.003$, partial $\eta^2 = 0.423$. Mean ± SE was higher at 14 days (1.964 ± 0.122) vs. 7 days (1.372 ± 0.122) (Fig. 5C).

Osteopontin

For *OPN* gene expression, there was no statistically significant interaction between group and time. Therefore, an analysis of the main effect for each factor was reported. As regards the main effect for group, there was no statistically significant difference in the mean values between the 4 groups [$F(3) = 1.252$, $p = 0.324$, partial $\eta^2 = 0.190$]. Mean ± SE was 1 ± 0.156 in negative control, 0.967 ± 0.156 in positive, 1.285 ± 0.156 in scaffold, and 1.287 ± 0.156 in scaffold/LLLT groups. The main effect analysis for time showed no statistically significant difference at 14 days vs. 7 days [$F(1) = 1.697$, $p = 0.211$, partial $\eta^2 = 0.096$]. Mean ± SE was slightly higher at 14 days (1.237 ± 0.111) vs. 7 days (1.033 ± 0.111) (Fig. 5D).

Collagen1α1

There was a statistically significant interaction between group and time on collagen1. Therefore, an analysis of simple main effects for each factor. As regards the simple main effect for group, there was a statistically significant difference in mean values between the 4 groups at each time point [$F(3, 16) = 1916.531$, $p < 0.001$, partial $\eta^2 = 0.997$ at 7-day time point, and $F(3, 16) = 1741.848$, $p < 0.001$, partial $\eta^2 = 0.997$ at 14-day time point]. At 7 days, pairwise comparisons revealed a statistically significant difference ($p < 0.001$) between negative control vs. all other 3 groups, but there was no statistically significant difference for all other pairwise comparisons ($p = 1.000$). At 14 days, there was a statistically significant difference ($p < 0.001$) between negative control vs. all other 3 groups, as well as positive control vs. scaffold/LLLT and scaffold vs. scaffold/LLLT, but there was no statistically significant difference between positive control vs. scaffold ($p = 1.000$).

As regards the simple main effect for time, there was a statistically significant difference in mean values between the 2 times in the scaffold/LLLT group only being higher at 14 days vs. 7 days [$F(1, 16) = 0.000$, $p = 1.000$, partial $\eta^2 = 0.000$ in negative control, $F(1, 16) = 2.148$, $p = 0.162$, partial $\eta^2 = 0.118$ in positive control, $F(1, 16) = 0.691$, $p = 0.418$, partial $\eta^2 = 0.041$ in scaffold, and $F(1, 16) = 48.517$, $p < 0.001$, partial $\eta^2 = 0.752$ in scaffold/LLLT groups] (Fig. 5E).

Discussion

Tissue engineering is an alternative solution to organ transplantation for repairing, replacing, or regenerating cells, tissues, or organs for the purpose of restoring impaired function caused by congenital defects, disease, trauma, or aging [36]. This regeneration is based on two essential components which are stem cells and scaffolds [37]. In addition, photobiomodulation was found to increase cellular metabolism, growth, and regeneration [18]. Therefore, in the current study, a tissue engineering complex composed of gingival-derived mesenchymal stem cells and nanocomposite scaffolds in conjunction with LLLT was formulated.

In the present study, GMSCs were successfully isolated and characterized regardless of the sensitive, critical isolation procedures required due to the high contamination risk which was attributed mainly to the high microbial oral flora especially in rats unlike humans who can keep good oral hygiene. Moreover, according to Kukreja et al. [38], MSC cultures can be contaminated at different stages during obtaining the tissue, transferring it to the working lab, or during the different culture procedures. To overcome this problem, meticulous wiping of the animal's skin with alcohol before starting surgical procedures and intraoral wiping with Betadine was performed. In addition, the obtained gingival tissues were immediately immersed in PBS supplemented with antibiotics before transferring to the working lab, and high infection control precautions were considered throughout the whole surgical and cultural procedures.

The constructed composite scaffold showed good biological, physical, chemical, and mechanical characteristics corresponding to its structure, as well as good hydrophilicity as detected by the water contact angle test. The peaks detected by FITR spectrometric analysis were comparable to other works of research [30–32]. Moreover, in accordance with the current study, similar studies showed high mechanical properties of different PCL/Alg-based scaffolds [33, 34]. In addition, the ultimate strain value of the developed scaffolds was similar to the normal bone range (2–30%) as reported by Osterhof et al. [35].

The increased cellular proliferation detected by MTT assay in the scaffold groups as compared to the control group indicates not only the biocompatibility of the fabricated scaffolds, but also its proliferative influence on the cells. This

inductive influence can be attributed to the porous scaffold structure which allows the diffusion of nutrients and cell products into and out of the scaffold and the proper mechanical and biological characters which simulate the extracellular matrix supporting the cells and promoting their proliferation and differentiation [39]. Moreover, in a previous study, the biocompatibility of similar PCL/Alg-based scaffolds was tested in vivo in a rabbit mandibular bone defect for 5 weeks with no adverse reactions [23].

However, there was insignificant weight loss and water absorption in the scaffold specimens through the 6 weeks of examination which is consistent with our previous study [23]. Similarly, Pattanashetti et al. [33] reported low degradation rates for cross-linked PCL/poly(vinyl alcohol):Alg. This may be attributed to the fact that PCL has low degradation and low water absorption rates [40]. Moreover, Shirehjini et al. [34] reported that scaffold degradability was reduced by increasing alginate concentration. Cross-linking also was found to reduce weight loss rates [40]. In addition, the electrospinning fabrication technique affects the material hydrophilicity reducing water absorption and hydrolytic degradability [41]. However, this can be considered beneficial for bone tissue engineering to allow enough time for bone regeneration and rearrangement before scaffold degradation.

In the present study, photobiostimulation protocol using InGaAs laser of 980 nm wavelength, 4.24 j/cm^2 energy density, and in a continuous mode was implicated. Different irradiation protocols were found in the literature including lower [42, 43] as well as higher [44, 45] energy densities. In the current study, an intermediate irradiation regimen as regards the energy density was selected. Moreover, repeated irradiations were performed for 150 s over 2 sessions separated by 75 s of rest with 48-h interval between consecutive irradiations to avoid any negative effects on the cells where according to Ohsugi et al. [46], increased irradiation powers or prolonged irradiation periods may cause cell damage or lead to inefficient treatment.

In addition, repeated irradiations seem to have a safe, better stimulatory effect on cell proliferation than single irradiation, which was confirmed by different studies, where according to Li et al. and Kreisler et al. [47, 48], a single dose of LLLT resulted in a short-term increase while multiple exposures caused maximal increase in MSC proliferation and osteogenic differentiation with no cytotoxic effects. In the same context, different human clinical trials also proved repeated irradiations with LLLT to be safe for application [49, 50].

In the current study, mineralization levels in the cultured media were detected by ARS and Von Kossa staining, while the osteoblastic differentiation of the GMSCs was assessed by determining the gene expression levels of an array of osteogenic-related genes (*ALP, RUNX2, COL1α1, OCN,* and *OPN*) through RT-qPCR.

Normally, there are three stages of bone development: proliferation, extracellular matrix (ECM) maturation, and mineralization. ARS marks the beginning of the mineralization step through quantification of red staining of mineralized calcium nodules [51]. Von Kossa also stains mineral deposits in the ECM [52]. *ALP* regulates ECM secretion prior to mineralization and also helps the formulation of Ca phosphate apatite crystals [53]. *RUNX2* is a very important transcription factor regulating early phases of osteoblastic differentiation, secreted at the highest level in immature osteoblasts, and decreased in mature osteoblasts [54]. *COL1α1* is upregulated during osteoblastic differentiation where it forms a fibrillary meshwork creating a complex 3D scaffold that supports cells [55]. *OPN* is a prominent bone matrix protein expressed at terminal phases of osteoblastic differentiation [56], and *OCN* is the most abundant non-collagenous bone matrix protein, produced by osteoblasts [57].

In the positive control group, GMSCs under appropriate induction showed good proliferation and osteogenic differentiation compared to the negative control cells. This agrees with the fact that gingival connective tissue–derived stem cells have self-renewal capacity, high potency, and immunomodulatory effects, together with osteogenic capacity and proved regenerative effects in animal bone defect models [58, 59].

However, the scaffold group expressed significantly higher proliferative and mineralization indices than the control groups which indicates its osteo-inductive influence where according to Jin and Kim [60], scaffolds, which consisted of electrospun nanofibers, exhibited a significantly high cell-seeding efficiency, due to the existence of embedded nanofibers. Additionally, coated scaffolds, consisting of PCL and various coating materials, such as collagen, alginate, and β-tricalcium phosphate, showed improved seeding, biological, and osteo-inductive characters when compared with pure PCL scaffolds.

These results coincide with our previous studies on the osteo-inductive effect of composite PCL/Alg-based nanoscaffolds on adipose-derived stem cells in vitro showing high ARS staining and *ALP* gene expression [22], and in vivo in rabbit mandibular bone defects aiding bone regeneration [23]. Concomitantly, in a study by Yu et al. [61], PCL/Alg composite scaffolds were reported to induce elevated expression levels of different osteogenic genes in progenitor cells such as *COL1α1* and *MEPE* (matrix extracellular phosphoglycoprotein) as well as chondrogenic genes such as *COL2α1* (collagen 2α1) and *ACAN* (aggrecan).

In group IV of the present study, photobiostimulation (InGaAs, 980 nm, 2.24 j/cm^2, repeated irradiations) of the GMSCs/scaffold complex efficiently enhanced the proliferation and osteogenic potential of the cells. Gao and Xing [62] postulated that the absorbed laser energy by intracellular

chromophores increased cellular metabolism, which stimulated the mitochondria to produce ATP, increase activity of DNA, and enhance RNA and protein synthesis. LLLT also suppresses inflammatory cytokines as tumor necrosis factor alpha (TNF-α, interleukins 1beta, 6, and 8) [63], and increases growth factors release as nerve growth factor (NGF), insulin-like growth factor 1 (IGF-1), fibroblast growth factor (FGF-2), and platelet-derived growth factor (PDGF) [64].

LLLT mainly affects the initial phases of bone regeneration, which are inflammatory, angio-mesenchymal, and bone formation phases. LLLT modulates the inflammatory response in vitro through a dual effect of WNT activation and NF-kβ signaling inhibition [65]. Regarding the angio-mesenchymal phase, LLLT induces an increase in VEGF, FGF, and PDGF in stem cells promoting their proliferation, osteogenic differentiation, and angiogenesis [20]. Considering the bone formation phase, LLLT has been found to increase the expression of different bone formation marker proteins, including BMP2, TGF-beta, and OCN [66]. Moreover, according to Huang et al. [67], irradiated scaffolds can absorb the laser beams and reflect physical waves that can affect the biological response of the loaded cells.

In the same context, Theocharidou et al. [68] reported better proliferative and odontogenic effect of LLLT (2 or 4 j/cm^2) on dental pulp stem cells seeded on bioceramic scaffolds as detected by MTT assay and elevated osteogenic gene expression; bone morphogenic protein-2 (*BMP2), RUNX2,* and *Osterix*. Corroborating our results, Huang et al. [67] detected good biostimulatory effect of LLLT (532 nm) on bone marrow stem cells (BMSCs) seeded on sheets of polylactic-co-glycolic acid (PLGA) mixed with graphene oxide. The study showed high proliferative and osteogenic influence in vitro as detected by elevated ALP activity, calcium content, and *OPN* gene expression, as well as in vivo in rat femoral bone defects. Similarly, in another study conducted by Abramovitch-Gottlib et al. [42], LLLT (He Ne, 632.8 nm) of MSCs on corraline 3D biomatrices resulted in increased mineralization levels revealing higher ALP activity, and elevated ARS and Von Kossa staining as compared to the non-irradiated groups.

ARS and Von Kossa staining in the present study detected significantly increased mineralization levels in the scaffold and irradiated groups than in the control groups. Relative gene expression levels of osteoblastic markers *ALP, RUNX2, and OCN* also showed significant increase in the positive control, scaffold, and irradiated scaffold groups respectively which is consistent with most literature as forementioned [22, 61, 67, 68]. However, *OPN* and *COL1α1* showed low expression levels. This may be attributed to the fact that some bone proteins are expressed at later stages of osteoblastic differentiation [69], while our experiment lasted only for 14 days.

On the other hand, Leonida et al. [70] tested the effect of irradiation (Nd:YAG, 1064 nm, 1.5W or 2.25W) on BMSCs seeded on 3D collagen scaffolds and reported enormous increase in mineralization as detected by alizarin red and proliferation rates on 7th day; however, on the 14th day, laser irradiation had no further effect on cellular proliferation which can be owed to the high wavelength and powers applied in this study.

In contrast to our results, Marques et al. [71] detected impaired protein secretion and even lower protein content in the media with LLLT. Also, in a study performed by Bouvet-Gerbettaz et al. [72], the influence of LLLT on BMSCs was detected by colony-forming unit fibroblasts (CFU-F) assay, and the non-irradiated group had a higher mean value of colonies than the irradiated group. It also did not enhance the differentiation of BMSCs to osteoblast or even to osteoclast. Concomitantly, other studies did not detect the stimulatory effect of LLLT on the proliferation or osteogenic differentiation of MSC [73–75].

These conflicting results may be attributed to the various parameters of laser application which markedly influence the required results, such as wavelength, light spectrum, energy density, and power level [76]. According to Peplow et al. [77], it is difficult to compare the different studies' results owing to the wide variation in irradiation parameters, methodology, and used cell type which directly affects the acquired biological effects.

In situ bone tissue engineering is a novel emerging field that comprises intraoperative cell isolation and seeding on scaffolds to construct a tissue engineering complex directly in the operating room. This represents a promising solution to evade the multiple steps and legal restrictions associated with introducing in vitro constructed tissue engineering grafts [78].

As per the contribution of the currently presented model to this novel field, gingival stem cells are considered good candidates for in situ tissue engineering where, as reported by Du et al. [79], gingival tissues can be easily accessed intraoperatively with minimally invasive procedures, and enzymatic digestion of gingival tissues can be performed in 2 h, which allows intraoperative seeding and application of in situ constructed scaffolds. Moreover, the cross-linked PCL/Alg-constructed scaffold in this study is slowly degradable, nanocomposite, synthetic/natural, polymeric complex, and according to Krasilnikova et al. [78], polymeric bioresorbable materials can be applied for in situ bone engineering purposes.

Among the limitations of this study is the limited follow-up periods for 7 and 14 days only. Also, the fabricated scaffold degradability was tested for 6 weeks. Longer

examination periods are required to detect its degradation behavior, stability, and biocompatibility in the long term. Moreover, there is a lack of comparison between different laser irradiation protocols which may have affected the results. In addition, the safety and efficacy of repeated LLLT exposure is a critical factor that warrants further investigations. Future in vivo experimental investigations are required to ensure the safety of the constructed regenerative complex in experimental animal models.

Conclusion

GMSCs are a rich, abundant, and easily accessible source of stem cells that possess a high differentiation potential. The fabricated PCL-NFs/Alg scaffold showed proper biological, physical, chemical, and mechanical characters, as well as efficient osteoconductive influence which qualify them to be an ideal scaffold for bone regeneration. LLLT has a cellular biostimulatory impact enhancing proliferative and osteogenic intracellular activities. GMSCs-PCL/Alg-LLLT complex can significantly enhance cellular proliferation, osteoblastic differentiation, and tissue mineralization through the upregulation of different osteogenic genes. Therefore, this cell/scaffold/LLLT triad can represent a promising choice for bone tissue engineering that needs to be further tested experimentally and clinically.

Abbreviations *MSCs*: Mesenchymal stem cells; *GMSCs*: Gingival mesenchymal stem cells; *BMMSCs*: Bone marrow mesenchymal stem cells; *PCL*: Polycaprolactone; *Alg*: Alginate; *LLLT*: Low-level laser therapy; $CaCl_2$: Calcium chloride; *SA*: Sodium alginate; *DCM*: Dichloromethane; *DMF*: N,N-Dimethylformamide; *PCL-NFs*: Polycaprolactone nanofibers; *SEM*: Scanning electron microscope; *EDX*: Energy-dispersive X-ray detector; *FTIR*: Fourier transform infrared; *PBS*: Phosphate-buffered saline; *D-MEM*: Dulbecco Modified Eagle Medium; *FBS*: Fetal bovine serum ; *MTT*: 3-(4,5-dimethylthiazol-2-yl)-2,5-diphenyltetrazolium bromide; *DMSO*: Dimethyl sulfoxide; *ARS*: Alizarin red S; $AgNO_3$: Silver nitrate; Na_2CO_3: Sodium carbonate; $Na_2S_2O_3$: Sodium thiosulfate; *dH2O*: Distilled water; *RT-qPCR*: Real-time quantitative polymerase chain reaction; *COL1α1*: Collagen 1α1; *BGLAP, OCN*: Osteocalcin; *SPP1, OPN*: Osteopontin; *ALP*: Alkaline phosphatase; *RUNX2*: Runt-related transcription factor 2; *GAPDH*: Glyceraldehyde-3 phosphate dehydrogenase; *ANOVA*: Analysis of variance; *ECM*: Extracellular matrix; *MEPE*: Matrix extracellular phosphoglycoprotein ; *COL2α1*: Collagen 2α1; *ACAN*: Aggrecan; *NGF* : Nerve growth factor; *IGF-1*: Insulin-like growth factor 1; *FGF-2*: Fibroblast growth factor 2; *PDGF*: Platelet-derived growth factor; *BMP2*: Bone morphogenic protein 2; *BMSCs*: Bone marrow stem cells; *PLGA*: Polylactic-co-glycolic acid; *CFU-F*: Colony-forming unit fibroblasts

Author Contribution EH: conceptualization; methodology; investigation; resources; writing—review and editing; project administration; funding acquisition. AE: methodology, investigation, data curation. ME: methodology, resources, visualization, validation. Z: methodology; formal analysis; writing—original draft. SY: investigation; resources; writing—original draft. IE: investigation, resources, supervision, validation. RE: conceptualization; methodology; investigation; writing—original draft; formal analysis. All authors read and approved the final manuscript.

Funding This study was funded by the General Administration for Scientific Research, Mansoura University, Egypt, with grant ID: Mu-Dent-20–1.

Data Availability All data generated or analyzed during this study are included in this published article.

Declarations

Ethical Approval All animal procedures were approved by the ethical committee of the Faculty of Dentistry, Mansoura University as part of the project entitled "Secretome analysis, proliferation and osteogenic differentiation of gingival derived stem cells seeded on nano-composite scaffold with and without LASER stimulation" (ID: A07080920, 8 September 2020) according to the guidelines of Mansoura University for animal care and use and following the ARRIVE guidelines (Animal Research: Reporting of In Vivo Experiments).

Consent for Publication Not applicable.

Competing Interests The authors declare no competing interests.

References

1. Su N, Villicana C, Yang F. Immunomodulatory strategies for bone regeneration: a review from the perspective of disease types. Biomaterials. 2022;286:121604. https://doi.org/10.1016/j.biomaterials.2022.121604.
2. Awad HA, O'Keefe RJ, Lee CH, Mao JJ. Chapter 83 - Bone tissue engineering: clinical challenges and emergent advances in orthopedic and craniofacial surgery. In: Lanza R, Langer R, Vacanti J, editors. Principles of tissue engineering. 4th ed. Boston: Academic Press; 2014. p. 1733–43. https://doi.org/10.1016/B978-0-12-398358-9.00083-5.
3. Ercal P, Pekozer GG, Kose GT. Dental stem cells in bone tissue engineering: current overview and challenges. Adv Exp Med Biol. 2018;1107:113–27. https://doi.org/10.1007/5584_2018_171.
4. Fawzy El-Sayed KM, Dörfer C, Fändrich F, Gieseler F, Moustafa MH, Ungefroren H. Adult mesenchymal stem cells explored in the dental field. Adv Biochem Eng Biotechnol. 2013;130:89–103. https://doi.org/10.1007/10_2012_151.
5. Cho MI, Garant PR. Development and general structure of the periodontium. Periodontol. 2000;2000(24):9–27. https://doi.org/10.1034/j.1600-0757.2000.2240102.x.
6. Zhang Q, Shi S, Liu Y, Uyanne J, Shi Y, Shi S, et al. Mesenchymal stem cells derived from human gingiva are capable of immunomodulatory functions and ameliorate inflammation-related tissue destruction in experimental colitis. J Immunol. 2009;183(12):7787–98. https://doi.org/10.4049/jimmunol.0902318.
7. Sun Q, Nakata H, Yamamoto M, Kasugai S, Kuroda S. Comparison of gingiva-derived and bone marrow mesenchymal stem cells for osteogenesis. J Cell Mol Med. 2019;23(11):7592–601. https://doi.org/10.1111/jcmm.14632.
8. Tomar GB, Srivastava RK, Gupta N, Barhanpurkar AP, Pote ST, Jhaveri HM, et al. Human gingiva-derived mesenchymal stem

cells are superior to bone marrow-derived mesenchymal stem cells for cell therapy in regenerative medicine. Biochem Biophys Res Commun. 2010;393(3):377–83. https://doi.org/10.1016/j.bbrc.2010.01.126.
9. Zhang Q, Shi S, Liu Y, Uyanne J, Shi Y, Shi S, et al. Mesenchymal stem cells derived from human gingiva are capable of immunomodulatory functions and ameliorate inflammation-related tissue destruction in experimental colitis. J Immunol. 2009;183(12):7787–98. https://doi.org/10.4049/jimmunol.0902318.
10. Ghassemi T, Shahroodi A, Ebrahimzadeh MH, Mousavian A, Movaffagh J, Moradi A. Current concepts in scaffolding for bone tissue engineering. Arch Bone Jt Surg. 2018;6(2):90–9. https://doi.org/10.22038/ABJS.2018.26340.1713.
11. Dai W, Kawazoe N, Lin X, Dong J, Chen G. The influence of structural design of PLGA/collagen hybrid scaffolds in cartilage tissue engineering. Biomaterials. 2010;31(8):2141–52. https://doi.org/10.1016/j.biomaterials.2009.11.070.
12. Balakrishnan B, Jayakrishnan A. Self-cross-linking biopolymers as injectable in situ forming biodegradable scaffolds. Biomaterials. 2005;26(18):3941–51. https://doi.org/10.1016/j.biomaterials.2004.10.005.
13. Farokhi M, JonidiShariatzadeh F, Solouk A, Mirzadeh H. Alginate based scaffolds for cartilage tissue engineering: a review. Int J Polym Mater Polym Biomater. 2020;69(4):230–47. https://doi.org/10.1080/00914037.2018.1562924.
14. Hany E, Yahia S, Elsherbeny MF, Salama NM, Ateia IM, Abou El-Khier NT, et al. Evaluation of the osteogenic potential of rat adipose-derived stem cells with different polycaprolactone/alginate-based nanofibrous scaffolds: an in vitro study. Stem Cell Investig 2020;7. https://doi.org/10.21037/sci-2020-015
15. Mansour AM, Yahia S, Elsayed HRH, El-Attar SA, Grawish ME, El-Hawary YM, et al. Efficacy of biocompatible trilayers nanofibrous scaffold with/without allogeneic adipose-derived stem cells on class II furcation defects of dogs' model. Clin Oral Investig. 2022;1–17. https://doi.org/10.1007/s00784-021-04222-x
16. AlGhamdi KM, Kumar A, Moussa NA. Low-level laser therapy: a useful technique for enhancing the proliferation of various cultured cells. Lasers Med Sci. 2012;27(1):237–49. https://doi.org/10.1007/s10103-011-0885-2.
17. Ginani F, Soares DM, Barreto MP, Barboza CA. Effect of low-level laser therapy on mesenchymal stem cell proliferation: a systematic review. Lasers Med Sci. 2015;30(8):2189–94. https://doi.org/10.1007/s10103-015-1730-9.
18. Carlos FP, de Paula Alves da Silva M, de Lemos Vasconcelos Silva Melo E, Costa MS, Zamuner SR. Protective effect of low-level laser therapy (LLLT) on acute zymosan-induced arthritis. Lasers Med Sci. 2014;29(2):757–63. https://doi.org/10.1007/s10103-013-1413-3
19. Amid R, Kadkhodazadeh M, Ahsaie MG, Hakakzadeh A. Effect of low level laser therapy on proliferation and differentiation of the cells contributing in bone regeneration. J Lasers Med Sci. 2014;5(4):163–70.
20. Bai J, Li L, Kou N, Bai Y, Zhang Y, Lu Y, et al. Low level laser therapy promotes bone regeneration by coupling angiogenesis and osteogenesis. Stem Cell Res Ther. 2021;12(1):432. https://doi.org/10.1186/s13287-021-02493-5.
21. Escudero JSB, Perez MGB, de Oliveira Rosso MP, Buchaim DV, Pomini KT, Campos LMG, et al. Photobiomodulation therapy (PBMT) in bone repair: a systematic review. Injury. 2019;50(11):1853–67. https://doi.org/10.1016/j.injury.2019.09.031.
22. Hany E, Yahia S, Elsherbeny MF, Salama NM, Ateia IM, Abou El-Khier NT, et al. Evaluation of the osteogenic potential of rat adipose-derived stem cells with different polycaprolactone/alginate-based nanofibrous scaffolds: an in vitro study. Stem Cell Investig. 2020;7:14. https://doi.org/10.21037/sci-2020-015.
23. Hany E, El-Wassefy N, Yahia S, Elkhier MA, El-Sherbiny IM. Characterization of a nanocomposite scaffold and assessment of its osteogenic influence in a rabbit mandibular bone defect model. J Oral Maxillofacial Surg, Med, Pathol. 2023;35(1):76–84. https://doi.org/10.1016/j.ajoms.2022.07.001.
24. Díaz E, Puerto I. In vitro degradation of PLCL/nHA biodegradable scaffolds. Polym-Plast Technol Eng. 2015;54(6):556–64. https://doi.org/10.1080/03602559.2014.961087.
25. Abd El-Latif N, Abdulrahman M, Helal M, Grawish ME. Regenerative capacity of allogenic gingival margin- derived stem cells with fibrin glue on albino rats' partially dissected submandibular salivary glands. Arch Oral Biol. 2017;82:302–9. https://doi.org/10.1016/j.archoralbio.2017.06.030.
26. Hanna H, Mir LM, Andre FM. In vitro osteoblastic differentiation of mesenchymal stem cells generates cell layers with distinct properties. Stem Cell Res Ther. 2018;9(1):203. https://doi.org/10.1186/s13287-018-0942-x.
27. Bernar A, Gebetsberger JV, Bauer M, Streif W, Schirmer M. Optimization of the alizarin red S assay by enhancing mineralization of osteoblasts. International Journal of Molecular Sciences [Internet]. 2023; 24(1). https://doi.org/10.3390/ijms24010723
28. Ball HC, Moussa FM, Mbimba T, Orman R, Safadi FF, Cooper LN. Methods and insights from the characterization of osteoprogenitor cells of bats (Mammalia: Chiroptera). Stem Cell Res. 2016;17(1):54–61. https://doi.org/10.1016/j.scr.2016.05.009.
29. Bonetti A, Contin M, Marchini M, Ortolani F. New insights on aortic valve interstitial cell calcification as revealed by von Kossa silver reactions adapted to electron microscopy. Eur J Histochem. 2023;67(2):10–1.
30. Sellimi S, Younes I, Ayed HB, Maalej H, Montero V, Rinaudo M, et al. Structural, physicochemical and antioxidant properties of sodium alginate isolated from a Tunisian brown seaweed. Int J Biol Macromol. 2015;72:1358–67. https://doi.org/10.1016/j.ijbiomac.2014.10.016.
31. Helmiyati H, Aprilliza M. Characterization and properties of sodium alginate from brown algae used as an ecofriendly superabsorbent. IOP Conf Ser: Mater Sci Eng. 2017;188:012019. https://doi.org/10.1088/1757-899X/188/1/012019.
32. Feng R, Song Z, Zhai G. Preparation and in vivo pharmacokinetics of curcumin-loaded PCL-PEG-PCL triblock copolymeric nanoparticles. Int J Nanomedicine. 2012;7:4089–98. https://doi.org/10.2147/ijn.S33607.
33 Pattanashetti NA, Achari DD, Torvi AI, Doddamani RV, Karidurag anavar MY. Development of multilayered nanofibrous scaffolds with PCL and PVA:NaAlg using electrospinning technique for bone tissue regeneration. Materialia. 2020;12:100826. https://doi.org/10.1016/j.mtla.2020.100826.
34. Shirehjini LM, Sharifi F, Shojaei S, Irani S. Poly-caprolactone nanofibrous coated with sol-gel alginate/ mesenchymal stem cells for cartilage tissue engineering. J Drug Delivery Sci Technol. 2022;74:103488. https://doi.org/10.1016/j.jddst.2022.103488.
35. Osterhoff G, Morgan EF, Shefelbine SJ, Karim L, McNamara LM, Augat P. Bone mechanical properties and changes with osteoporosis. Injury. 2016;47:S11–20. https://doi.org/10.1016/S0020-1383(16)47003-8.
36. Mason C, Dunnill P. A brief definition of regenerative medicine. Regen Med. 2008;3(1):1–5. https://doi.org/10.2217/17460751.3.1.1.
37. Zhang L, Webster TJ. Nanotechnology and nanomaterials: promises for improved tissue regeneration. 2009;4(1):66-80. https://doi.org/10.1016/j.nantod.2008.10.014
38. Kukreja BJ, Bhat KG, Kukreja P, Kumber VM, Balakrishnan R, Govila V. Isolation and immunohistochemical characterization of periodontal ligament stem cells: a preliminary study. J Indian Soc Periodontol. 2021;25(4):295–9. https://doi.org/10.4103/jisp.jisp_442_20.

39. Seyedjafari E, Soleimani M, Ghaemi N, Sarbolouki MN. Enhanced osteogenic differentiation of cord blood-derived unrestricted somatic stem cells on electrospun nanofibers. J Mater Sci - Mater Med. 2011;22:165–74. https://doi.org/10.1007/s10856-010-4174-6.
40. Yahia S, Khalil IA, El-Sherbiny IM. Sandwich-like nanofibrous scaffolds for bone tissue regeneration. ACS Appl Mater Interfaces. 2019;11(32):28610–20. https://doi.org/10.1021/acsami.9b06359.
41. Bölgen N, Menceloğlu YZ, Acatay K, Vargel I, Pişkin E. In vitro and in vivo degradation of non-woven materials made of poly(epsilon-caprolactone) nanofibers prepared by electrospinning under different conditions. J Biomater Sci Polym Ed. 2005;16(12):1537–55. https://doi.org/10.1163/156856205774576655.
42. Abramovitch-Gottlib L, Gross T, Naveh D, Geresh S, Rosenwaks S, Bar I, et al. Low level laser irradiation stimulates osteogenic phenotype of mesenchymal stem cells seeded on a three-dimensional biomatrix. Lasers Med Sci. 2005;20(3):138–46. https://doi.org/10.1007/s10103-005-0355-9.
43. Etemadi A, Faghih A, Chiniforush N. Effects of photobiomodulation therapy with various laser wavelengths on proliferation of human periodontal ligament mesenchymal stem cells. Photochem Photobiol. 2022;98(5):1182–9. https://doi.org/10.1111/php.13588.
44. İslam A, Özverel CS, Yilmaz HG. Comparative evaluation of low-level laser therapy on proliferation of long-term cryopreserved human dental pulp cells isolated from deciduous and permanent teeth. Lasers Med Sci. 2021;36(2):421–7. https://doi.org/10.1007/s10103-020-03090-3.
45. Gkogkos AS, Karoussis IK, Prevezanos ID, Marcopoulou KE, Kyriakidou K, Vrotsos IA. Effect of Nd: YAG low level laser therapy on human gingival fibroblasts. Int J Dent. 2015. https://doi.org/10.1155/2015/258941.
46. Ohsugi Y, Niimi H, Shimohira T, Hatasa M, Katagiri S, Aoki A, et al. In vitro cytological responses against laser photobiomodulation for periodontal regeneration. Int J Mol Sci. 2020;21(23). https://doi.org/10.3390/ijms21239002
47. Li WT, Leu YC, Wu JL. Red-light light-emitting diode irradiation increases the proliferation and osteogenic differentiation of rat bone marrow mesenchymal stem cells. Photomed Laser Surg. 2010;28(Suppl 1):S157–65. https://doi.org/10.1089/pho.2009.2540.
48. Kreisler M, Christoffers AB, Willershausen B, D'Hoedt B. Effect of low-level GaAlAs laser irradiation on the proliferation rate of human periodontal ligament fibroblasts: an in vitro study. J Clin Periodontol. 2003;30(4):353–8. https://doi.org/10.1034/j.1600-051x.2003.00001.x.
49. Lanzafame RJ, Blanche RR, Bodian AB, Chiacchierini RP, Fernandez-Obregon A, Kazmirek ER. The growth of human scalp hair mediated by visible red light laser and LED sources in males. Lasers Surg Med. 2013;45(8):487–95. https://doi.org/10.1002/lsm.22173.
50. Ahmad MA, Moganan M, A Hamid MS, Sulaiman N, Moorthy U, Hasnan N, et al. Comparison between low-level and high-intensity laser therapy as an adjunctive treatment for knee osteoarthritis: a randomized, double-blind clinical trial. Life. 2023; 13(7). https://doi.org/10.3390/life13071519
51. GurelPekozer G, Ramazanoglu M, Schlegel KA, Kok FN, Torun KG. Role of STRO-1 sorting of porcine dental germ stem cells in dental stem cell-mediated bone tissue engineering. Artif Cells Nanomed Biotechnol. 2018;46(3):607–18. https://doi.org/10.1080/21691401.2017.1332637.
52. Wang YH, Liu Y, Maye P, Rowe DW. Examination of mineralized nodule formation in living osteoblastic cultures using fluorescent dyes. Biotechnol Prog. 2006;22(6):1697–701. https://doi.org/10.1021/bp060274b.
53. Mizuno M, Kuboki Y. Osteoblast-related gene expression of bone marrow cells during the osteoblastic differentiation induced by type I collagen. J Biochem. 2001;129(1):133–8. https://doi.org/10.1093/oxfordjournals.jbchem.a002824.
54. Komori T. Regulation of proliferation, differentiation and functions of osteoblasts by Runx2. Int J Mol Sci. 2019;20(7). https://doi.org/10.3390/ijms20071694
55. Frantz C, Stewart KM, Weaver VM. The extracellular matrix at a glance. J Cell Sci. 2010;123(Pt 24):4195–200. https://doi.org/10.1242/jcs.023820.
56 Mizerska-Kowalska M, Sławińska-Brych A, Kaławaj K, Żurek A, Pawińska B, Rzeski W, et al. Betulin promotes differentiation of human osteoblasts in vitro and exerts an osteoinductive effect on the hFOB 1.19 cell line through activation of JNK, ERK1/2, and mTOR Kinases. Molecules. 2019;24(14):2637. https://doi.org/10.3390/molecules24142637.
57. Wang JS, Mazur CM, Wein MN. Sclerostin and osteocalcin: candidate bone-produced hormones. Front Endocrinol (Lausanne). 2021;12:584147. https://doi.org/10.3389/fendo.2021.584147.
58. Kandalam U, Kawai T, Ravindran G, Brockman R, Romero J, Munro M, et al. Predifferentiated gingival stem cell-induced bone regeneration in rat alveolar bone defect model. Tissue Eng Part A. 2021;27(5–6):424–36. https://doi.org/10.1089/ten.tea.2020.0052.
59. Al-Qadhi G, Soliman M, Abou-Shady I, Rashed L. Gingival mesenchymal stem cells as an alternative source to bone marrow mesenchymal stem cells in regeneration of bone defects: in vivo study. Tissue Cell. 2020;63:101325. https://doi.org/10.1016/j.tice.2019.101325.
60. Jin G, Kim G. Multi-layered polycaprolactone–alginate–fucoidan biocomposites supplemented with controlled release of fucoidan for bone tissue regeneration: fabrication, physical properties, and cellular activities. J Soft Matter. 2012;8(23):6264–72. https://doi.org/10.1039/C2SM07256D.
61. Yu J, Lee S, Choi S, Kim KK, Ryu B, Kim CY, et al. Fabrication of a polycaprolactone/alginate bipartite hybrid scaffold for osteochondral tissue using a three-dimensional bioprinting system. Polymers [Internet]. 2020; 12(10). https://doi.org/10.3390/polym12102203
62. Gao X, Xing D. Molecular mechanisms of cell proliferation induced by low power laser irradiation. J Biomed Sci. 2009;16(1):4. https://doi.org/10.1186/1423-0127-16-4.
63. Shiba H, Tsuda H, Kajiya M, Fujita T, Takeda K, Hino T, et al. Neodymium-doped yttrium-aluminium-garnet laser irradiation abolishes the increase in interleukin-6 levels caused by peptidoglycan through the p38 mitogen-activated protein kinase pathway in human pulp cells. J Endod. 2009;35(3):373–6. https://doi.org/10.1016/j.joen.2008.11.028.
64. Safavi SM, Kazemi B, Esmaeili M, Fallah A, Modarresi A, Mir M. Effects of low-level He-Ne laser irradiation on the gene expression of IL-1beta, TNF-alpha, IFN-gamma, TGF-beta, bFGF, and PDGF in rat's gingiva. Lasers Med Sci. 2008;23(3):331–5. https://doi.org/10.1007/s10103-007-0491-5.
65. Sakata S, Kunimatsu R, Tsuka Y, Nakatani A, Gunji H, Yanoshita M, et al. High-frequency near-infrared diode laser irradiation suppresses IL-1β-induced inflammatory cytokine expression and NF-κB signaling pathways in human primary chondrocytes. Lasers Med Sci. 2022;37(2):1193–201. https://doi.org/10.1007/s10103-021-03371-5.
66. de Oliveira GJPL, Aroni MAT, Pinotti FE, Marcantonio E, Marcantonio RAC. Low-level laser therapy (LLLT) in sites grafted with osteoconductive bone substitutes improves osseointegration. Lasers Med Sci. 2020;35(7):1519–29. https://doi.org/10.1007/s10103-019-02943-w.
67. Huang Z, Xu J, Chen J, Chen H, Wang H, Huang Z, et al. Photoacoustic stimulation promotes the osteogenic differentiation of bone mesenchymal stem cells to enhance the repair of bone defect. Sci Rep. 2017;7(1):15842. https://doi.org/10.1038/s41598-017-15879-4.
68. Theocharidou A, Bakopoulou A, Kontonasaki E, Papachristou E, Hadjichristou C, Bousnaki M, et al. Odontogenic differentiation

and biomineralization potential of dental pulp stem cells inside Mg-based bioceramic scaffolds under low-level laser treatment. Lasers Med Sci. 2017;32(1):201–10. https://doi.org/10.1007/s10103-016-2102-9.
69. Niknam Z, Golchin A, Rezaei-Tavirani M, Ranjbarvan P, Zali H, Omidi M, et al. Osteogenic differentiation potential of adipose-derived mesenchymal stem cells cultured on magnesium oxide/polycaprolactone nanofibrous scaffolds for improving bone tissue reconstruction. Adv Pharm Bull. 2022;12(1):142–54. https://doi.org/10.34172/apb.2022.015.
70. Leonida A, Paiusco A, Rossi G, Carini F, Baldoni M, Caccianiga G. Effects of low-level laser irradiation on proliferation and osteoblastic differentiation of human mesenchymal stem cells seeded on a three-dimensional biomatrix: in vitro pilot study. Lasers Med Sci. 2013;28(1):125–32. https://doi.org/10.1007/s10103-012-1067-6.
71. Marques MM, Pereira AN, Fujihara NA, Nogueira FN, Eduardo CP. Effect of low-power laser irradiation on protein synthesis and ultrastructure of human gingival fibroblasts. Lasers Surg Med. 2004;34(3):260–5. https://doi.org/10.1002/lsm.20008.
72. Bouvet-Gerbettaz S, Merigo E, Rocca JP, Carle GF, Rochet N. Effects of low-level laser therapy on proliferation and differentiation of murine bone marrow cells into osteoblasts and osteoclasts. Lasers Surg Med. 2009;41(4):291–7. https://doi.org/10.1002/lsm.20759.
73. Rahmati A, Abbasi R, Najafi R, Rezaei-soufi L, Karkehabadi H. Effect of diode low level laser and red light emitting diode irradiation on cell proliferation and osteogenic/odontogenic differentiation of stem cells from the apical papilla. BMC Oral Health. 2022;22(1):543. https://doi.org/10.1186/s12903-022-02574-8.
74. Gholami L, Parsamanesh G, Shahabi S, Jazaeri M, Baghaei K, Fekrazad R. The effect of laser photobiomodulation on periodontal ligament stem cells. Photochem Photobiol. 2021;97(4):851–9. https://doi.org/10.1111/php.13367.
75. Pereira LO, Longo JP, Azevedo RB. Laser irradiation did not increase the proliferation or the differentiation of stem cells from normal and inflamed dental pulp. Arch Oral Biol. 2012;57(8):1079–85. https://doi.org/10.1016/j.archoralbio.2012.02.012.
76. Soares DM, Ginani F, Henriques ÁG, Barboza CA. Effects of laser therapy on the proliferation of human periodontal ligament stem cells. Lasers Med Sci. 2015;30(3):1171–4. https://doi.org/10.1007/s10103-013-1436-9.
77. Peplow PV, Chung TY, Baxter GD. Laser photobiomodulation of proliferation of cells in culture: a review of human and animal studies. Photomed Laser Surg. 2010;28(Suppl 1):S3-40. https://doi.org/10.1089/pho.2010.2771.
78. Krasilnikova OA, Baranovskii DS, Yakimova AO, Arguchinskaya N, Kisel A, Sosin D, et al. Intraoperative creation of tissue-engineered grafts with minimally manipulated cells: new concept of bone tissue engineering in situ. Bioengineering (Basel). 2022;9(11). https://doi.org/10.3390/bioengineering9110704
79. Du L, Yang P, Ge S. Isolation and characterization of human gingiva-derived mesenchymal stem cells using limiting dilution method. J Dent Sci. 2016;11(3):304–14. https://doi.org/10.1016/j.jds.2016.03.010.

Authors and Affiliations

Eman Hany[1] · Ahmed A. Emam[2] · Mohamed G. Elbeltagy[3] · Mahmoud M. Zakaria[4] · Sarah Yahia[5] · Ibrahim M. El-Sherbiny[5] · Rana El-Qashty[1]

✉ Eman Hany
eman_haney@mans.edu.eg

Ahmed A. Emam
ahmedabdou@mans.edu.eg

Mohamed G. Elbeltagy
MohamedGamalMohamed.Elbeltagy@uk-essen.de

Mahmoud M. Zakaria
mahmoudzakaria@mans.edu.eg

Sarah Yahia
smoustafa@zewailcity.edu.eg

Ibrahim M. El-Sherbiny
ielsherbiny@zewailcity.edu.eg

Rana El-Qashty
Dr_rana_nagah@mans.edu.eg

1 Oral Biology Department, Faculty of Dentistry, Mansoura University, Mansoura, Egypt

2 Medical Experimental Research Center (MERC), Faculty of Medicine, Mansoura University, Mansoura, Egypt

3 Present Address: Institute for Transfusion Medicine, University Hospital Essen, University of Duisburg-Essen, Essen, Germany

4 Urology & Nephrology Center, Faculty of Medicine, Mansoura University, Mansoura, Egypt

5 Nanomedicine Research Labs, Center of Materials Sciences, Zewail City of Science and Technology, Giza, Egypt